Cement and Concrete Research 41 (2011) 77–89

Contents lists available at ScienceDirect

Cement and Concrete Research

journal homepage: http://ees.elsevier.com/CEMCON/default.asp

Desiccation shrinkage of cementitious materials as an aging, poroviscoelastic response

Zachary C. Grasley *, Chin K. Leung

Zachry Department of Civil Engineering, Texas A&M University, College Station, TX 77845, USA

ARTICLE INFO

Article history:
Received 26 February 2010
Accepted 17 September 2010

Keywords:
Shrinkage (C)
Creep (C)
Humidity (A)
Poroelastic

ABSTRACT

This paper describes and evaluates a new model that utilizes aging poroviscoelasticity for predicting the shrinkage of cementitious materials induced by loss of moisture from the pore structure (i.e. desiccation). The new model incorporates well-accepted mechanisms for desiccation shrinkage and accounts for the effect of changing concentrations of dissolved species in the pore fluid. Additionally, the model is used to interpret viscoelastic behavior during the drying process via comparisons of model predictions with measured shrinkage of hardened portland cement paste. It was found that while a poroelastic model under predicts the measured shrinkage, the poroviscoelastic model significantly over predicts the shrinkage unless intrinsic aging of the C–S–H gel is included in the model.

1. Introduction

Shrinkage of concrete due to loss of evaporable pore water can lead to crack development and reduction in durability. Concrete shrinkage due to loss of pore water is often subdivided into autogenous and drying shrinkage, with autogenous shrinkage associated with loss of evaporable pore water through consumption in the hydration reaction, and drying shrinkage associated with loss of evaporable pore water through transport to an open boundary. While often divided, autogenous and drying shrinkage only differ in how the pore water is removed; mechanistically, the shrinkage deformations are identical. Therefore, this paper treats modeling of desiccation shrinkage, where desiccation refers to either self-desiccation through the hydration reaction, or desiccation due to loss of pore water/vapor through an open boundary (or a combination of both types of desiccation). The objective of this paper is to derive a new desiccation shrinkage model for cementitious materials and to compare model predictions with measured shrinkage of hardened cement paste (HCP).

Shrinkage due to loss of evaporable pore water from cementitious materials has typically been attributed to three primary mechanisms (or driving forces) [1,2]:

1. changes in capillary pressure,
2. changes in disjoining pressure, and
3. changes in the surface energy of the solid phase.

Most modeling efforts have focused on changes in pore fluid pressure associated with capillary pressure and disjoining pressure, which are simultaneously determined from changes in relative humidity (*RH*) and/or temperature using the well-known Kelvin–Laplace relationship [2,3]. Change in the surface energy of the solid phase is an inverse function of the degree of saturation, and is thus thought to be most prominent at low levels of saturation [1].

Poroelasticity has been successfully used to model deformation of HCP and other porous materials caused by pore fluid pressure changes (see e.g. [4–9]). Bentz et al. [10] modeled the drying shrinkage of partially saturated porous Vycor® glass rods using a poroelastic model. The approach involved the use of a modified version of Biot's elastic constitutive equation[1] (using a saturation factor) to account for the partial saturation conditions inherent to drying. Coussy et al. [4,12] formalized the use of a saturation factor based on the work of Bishop [13] and derived an "effective pore pressure" to be used with poroelasticity to predict shrinkage of cement-based materials. The effective pore pressure included changes in pore fluid pressure (associated with mechanisms 1 and 2 above) and the interfacial energy of the system (associated with mechanism 3 above). Lura et al. [14–16], Coussy et al. [4], Weiss et al. [17], and Rougelot et al. [18] have used the Kelvin–Laplace equation and poroelasticity to model shrinkage of cementitious materials as a function of *RH*. Lura et al. noted good agreement between measured and modeled shrinkage for specimens at higher *RH*; however, the model under predicted shrinkage at lower *RH*, and the difference was attributed to viscoelastic effects not accounted for in the model.

* Corresponding author. Tel.: +1 979 845 9961; fax: +1 979 458 0780.
E-mail address: zgrasley@civil.tamu.edu (Z.C. Grasley).

0008-8846/$ – see front matter © 2010 Elsevier Ltd. All rights reserved.
doi:10.1016/j.cemconres.2010.09.008

[1] Bentz et al. [10] refer to the work of Mackenzie [11] (which predates Biot) in their paper. Mackenzie's model is identical to that of Biot's isotropic poroelastic model, but Mackenzie overly restricts the model to bodies with spherical pores whereas Biot makes no restriction regarding pore geometry.

At early ages in particular, HCP exhibits significant viscoelastic effects [19,20]. In addition, the viscoelastic properties are subject to aging, particularly at early age [20,21]. As with externally applied loads, it is reasonable to include both viscoelastic effects and aging in a desiccation shrinkage model. Recent work has indicated that the viscoelastic behavior of cementitious materials is primarily associated with movement of C–S–H globules or particles under local stress [22,23]. Because of the state of partial saturation inherent to the desiccation process, drying will induce local shear stress in the C–S–H even though the pressure in the gaseous and liquid phases in the pore network are each in a state of hydrostatic pressure. Therefore, it is reasonable to assume creep constitutes a component of shrinkage. In addition, there is experimental evidence indicating continued desiccation shrinkage even at constant internal *RH* (i.e. constant internal pore pressure) [24]. It is also reasonable to include aging of the viscoelastic effects in a desiccation shrinkage model. Aging is likely attributable to increased formation of hydration products due to hydration [25,26] and increased polymerization [22] or compaction [27] of the C–S–H as a function of time[2]. Each of these aging mechanisms would affect the response of a porous cementitious material to changes in pore fluid pressure. Additionally, C–S–H polymerization and compaction has been shown to increase as a result of the drying process [28], making aging even more critical for modeling desiccation shrinkage. Previous research [29,30] has modeled shrinkage of HCP as a viscoelastic response, but did not include aging effects or poromechanical principles.

The approach to modeling desiccation shrinkage taken in this paper incorporates both poromechanics and aging viscoelasticity. Grasley [24] modeled autogenous shrinkage of HCP with a porovis-coelastic model, but uncertainties in the internal *RH* measurement and the use of a saturation function from a model instead of direct measurement led to a discrepancy between measured shrinkage and model prediction. Additionally, Grasley's model was only applicable to the high *RH* regime since changes in interfacial energy were neglected. This paper presents a desiccation shrinkage model for cementitious materials incorporating all commonly accepted mechanisms for desiccation shrinkage as well as aging viscoelastic effects using a poromechanical framework. Additionally, the effect of changing pore solution concentrations during desiccation is directly incorporated into the shrinkage model.

2. Model derivation

The model derived is essentially an extension of the poroelastic desiccation shrinkage model derived by Coussy et al. [4]. The two primary additions to the Coussy model are the inclusion of the effect of dissolved species in the pore fluid on effective pore pressure, and the addition of aging viscoelasticity to the constitutive model. The following subsections detail the model derivation.

2.1. Constitutive model

2.1.1. Poromechanics for partially saturated porous media

Poromechanics models the response of porous media associated with coupled solid–pore fluid interaction, and was first proposed by Biot [31]. Assuming small displacement gradients, the constitutive equation for a linear elastic isotropic porous solid is

$$\varepsilon_{ij} = \frac{1}{2G_p}\left(\sigma_{ij} - \frac{\nu_p}{1+\nu_p}\delta_{ij}\sigma_{kk}\right) - \frac{b}{3K_p}P\delta_{ij}, \tag{1}$$

where ε_{ij} are components of the strain tensor, σ_{ij} are components of the externally applied (to the boundary of the porous body) stress tensor, σ_{kk} is the trace of the stress tensor, δ_{ij} is the Kronecker delta, G_p is the shear modulus of the porous body, K_p is the bulk modulus of the porous body, P is the pore fluid pressure, and b is the Biot–Willis effective stress coefficient given by $1-K_p/K_s$, where K_s is the bulk modulus of the solid phase comprising the skeleton of the porous body.

An averaged pore fluid pressure approach has long been used to model the effect of coexisting fluids in porous media [13]; indeed, this approach is within the framework of classical mixture theory (see, e.g. [32]). For the particular case of pore water and air, pore water would exert a pressure (negative) when the local internal *RH* is lower than 100%[3], and air would exert a pressure dependent on the concentrations of gases present [33]. Assuming porosity is invariant to load or that the gas-filled and liquid filled pores deform uniformly [34], the pore liquid pressure and the pressure in the gaseous phase can be combined with the relative volume fractions (of the pore space) of the pore liquid and gases to define an average pore pressure as

$$P_{avg} = (1-S)P_g + SP_l = -SP_c + P_g \approx -SP_c. \tag{2}$$

Here, $P_c = P_g - P_l$ is the capillary pressure, S is the saturation factor of the liquid phase ($0 \le S \le 1$), P_l is the pore liquid pressure, and P_g is the pressure of the gaseous phase. In the drying case, since the magnitude of the gaseous pressure is minimal in comparison with the liquid pressure magnitude, $P_g \approx 0$ and Eq. (2) simplifies as shown.

As shrinkage of cementitious materials is purely dilatational, it is convenient to simplify Eq. (1) for volumetric response such that

$$\varepsilon = \frac{\sigma}{K_p} + P\left(\frac{1}{K_p} - \frac{1}{K_s}\right), \tag{3}$$

where $\varepsilon = \varepsilon_{ii} = \varepsilon_{11} + \varepsilon_{22} + \varepsilon_{33}$ is the volumetric strain and σ is the externally applied volumetric stress (i.e. $\sigma_{ii}/3$). If the effects of interfaces within the pore network are negligible, an elastic model for predicting volumetric shrinkage can be obtained by replacing P in Eq. (3) with P_{avg} and setting $\sigma = 0$. However, as noted by Coussy et al. [4,12], it is important to include interfacial effects, particularly at lower *RH*.

An alternative approach for quantifying the effect of partial saturation on shrinkage of porous materials using poromechanics has recently been derived independently by Rougelot et al. [18] and Vlahinic et al. [35]. The approach involves matching the pore volume to the volume of pores filled with liquid at any point in time — i.e. in Eq. (2), $S = 1$ at all times such that $P_{avg} = P_l$. The effect of empty porosity (caused by reductions in liquid saturation due to drying) is accounted for by incorporation of the empty porosity into the "solid phase" such that K_s is a function of the drying state. As pores desiccate, K_s decreases due to the increased compressibility caused by incorporation of highly compressible gases into the volume of "solid" material. A primary limitation of this alternative approach is that incorporation of changes in interfacial energy becomes convoluted such that the models are likely to only be valid at high *RH* where capillary pressure is dominant. Additionally, whereas K_s may typically be considered as elastic [24], the incorporation of porosity into the solid phase means that shear stresses will be present in the "solid" material regardless of the externally applied stress state. Therefore, K_s most certainly will be viscoelastic, further complicating the analysis. In the average pore pressure method, only K_p must be considered as viscoelastic.

[2] Note that the literature is split in the definition of aging — some regard aging as a chemical process independent of hydration, whereas some regard aging as the combined effect of hydration and other chemical processes on mechanical properties. We have adopted the latter definition in this paper.

[3] For pore solution with dissolved species, the negative pressure will not develop until the internal *RH* is reduced below an equilibrium level dictated by the dissolved species concentration. See Section 2.2.1 for details.

In the model to be derived herein, the average pore pressure method will be adopted such that Eqs. (2) and (3) form the basis for the constitutive model. In the case of desiccation, $P_{avg}<0$. Additionally, we neglect any effect of P_{avg} on the pore structure, which is considered to change strictly as a function of hydration.

2.1.2. Aging viscoelasticity of cementitious materials

Eq. (3) is valid for a non-aging elastic material. However, HCP is viscoelastic and also exhibits aging of both elastic and viscoelastic properties; neither effect is accounted for with the theory of poroelasticity alone. Aging viscoelasticity is particularly significant at early ages, where creep may decrease by up to 5 times in magnitude between the ages of 1 and 28 days [20].

The most basic uniaxial constitutive equation for an aging, linear viscoelastic material is

$$\varepsilon_{11}(t,t') = \int_0^t J_p(t,t')\frac{\partial\sigma_{11}(t')}{\partial t'}dt', \tag{4}$$

where $\varepsilon_{11}(t,t')$ is the viscoelastic axial strain at time t caused by the stress applied at time t', $J_p(t,t')$ is the uniaxial viscoelastic compliance of the porous body, and $\sigma_{11}(t')$ is the axial stress. Aging of early age HCP is due in part to the hydration reaction, which results in gradual solidification of the load-bearing hydration products. Therefore, to account for aging in the desiccation shrinkage model, the solidification theory developed by Bazant [25] and Carol and Bazant [26] is adopted. For solidifying materials, the aging viscoelastic compliance can be expressed as

$$J_p(t,t') = \frac{1}{E_p v(t')} + \int_{t'}^t \frac{1}{v(\theta)}\frac{\partial J_s(\theta-t')}{\partial\theta}d\theta, \tag{5}$$

where $J_p(t,t')$ is the viscoelastic compliance of the bulk porous material, $J_s(t)$ is the non-aging viscoelastic compliance of the solidifying material, E_p is the elastic Young's modulus of the porous material, $v(t)$ is the solidification aging function, and θ is a dummy time variable of integration. Applying an aging function to the uniaxial compliance (while assuming a non-aging viscoelastic Poisson's ratio) implies that the aging of dilatational and deviatoric moduli proceed at identical rates. The importance of this implication is discussed further in §5.

Grasley and Lange [20] demonstrated that solidification alone is unable to fully account for the aging process of early age cementitious materials undergoing a reduction in internal *RH*. In agreement with their findings, other researchers have suggested that drying can increase aging either through increased polymerization [28] or packing density [27] of the C–S–H. Since desiccation shrinkage inherently involves reductions in internal *RH*, it is plausible that additional aging mechanisms beyond solidification are active. Both suggested mechanisms for additional aging (polymerization and packing) represent aging of the solid phase of the material (i.e. $J_s(t)\rightarrow J_s(t,t')$).

Grasley and Lange suggested using the time-shift approach for modeling intrinsic aging of the solidifying solid phase of the porous body (i.e. aging of the C–S–H) [20]. The time-shift approach has been used extensively in the polymers research area, but has seen limited use as a tool to evaluate cement paste or concrete. However, Vichit-Vadakan and Scherer [21] suggested that the shape of the relaxation function was preserved during aging, and successfully applied the time-shift technique to cement pastes to account for the aging effect on short-term early age stress relaxation. This approach implied that a change in the relaxation response of the material could be accounted for purely by a change in the viscoelastic retardation (or relaxation) times [21].

The time-shift approach to model aging viscoelasticity is analogous to the time–temperature superposition principle first derived by Morland and Lee [36]. This principle states that the effect of a change in temperature is to cause either an increase or decrease in the retardation or relaxation times. The result is simply a shift in the compliance or moduli functions along the log time axis without changing the shape of the curves. Materials that maintain the shape of the relaxation or compliance functions on the log time scale with change in temperature are called 'thermorheologically simple' [37]. Analogously, we consider the solidifying C–S–H gel to maintain the shape of the relaxation or compliance functions on the log time scale with a change in material age. Therefore, the aging of $J_s(t)$ may be accounted for by simply shifting the real time on the log axis, where the shifting accounts for the age of the material and the shape of the compliance function does not change.

The shift constants for each age may be recorded and fit to a function A_t such as

$$A_t = \left(\frac{t_{ref}}{t}\right)^{\mu}, \tag{6}$$

where t_{ref} is the reference master age at which the compliance function is fitted and to which the other ages are shifted, t is the current age, and μ is a fitting parameter that defines the rate of aging [38]. The uniaxial constitutive equation for an aging, solid material may then be written as [36]

$$\varepsilon_{11}(t) = \int_0^t J_s(\xi(t)-\xi(t'))\frac{\partial\sigma_{11}(t')}{\partial t'}dt' + \varepsilon^f(t)\delta_{ij}, \tag{7}$$

where ξ is a pseudo-time and $\xi(t)-\xi(t')$ is expressed as

$$\xi(t)-\xi(t') = \int_{t'}^t \frac{dt''}{A_t(t'')}, \tag{8}$$

where t'' is a dummy time integration variable. A combination of Eqs. (6) and (8) and subsequent integration results in

$$\xi(t)-\xi(t') = \left(\frac{\left(t+t_{ref}\right)^{1+\mu}-\left(t'+t_{ref}\right)^{1+\mu}}{1+\mu}\right)t_{ref}^{-\mu}. \tag{9}$$

By replacing $J_s(t)$ in Eq. (5) with $J_s(\xi(t))$, one obtains

$$J_p(t,t') = \frac{1}{E_p v(t')} + \int_{t'}^t \frac{1}{v(\theta)}\frac{\partial J_s\{\xi(\theta)-\xi(t')\}}{\partial\theta}d\theta, \tag{10}$$

which is a uniaxial viscoelastic compliance function that simultaneously accounts for aging due to solidification and intrinsic aging of the solidifying C–S–H gel (through the time-shift).

2.1.3. Aging, poroviscoelastic constitutive model

For a linear viscoelastic, non-aging material, Eq. (3) becomes

$$\varepsilon(t) = \int_0^t \frac{\partial\sigma(t')}{\partial t'}B_p(t-t') + \frac{\partial P(t')}{\partial t'}\left(B_p(t-t')-\frac{1}{K_s}\right)dt', \tag{11}$$

where it is assumed that K_s has negligible time-dependency, and $B_p(t)$ is the dilatational viscoelastic compliance.

For an isotropic, linear viscoelastic material, $B_p(t)$ may be determined from $J_p(t)$ and the viscoelastic Poisson's ratio of the porous body $\nu_p(t)$ in the Laplace Transform domain according to

$$\overline{B}_p(s) = \frac{1}{s^2\overline{K}_p(s)} = 3\left(1-2s\overline{\nu}_p(s)\right)\overline{J}(s), \tag{12}$$

where the overbars denote the Laplace Transformed quantity and s is the transform variable. As suggested by Grasley and Lange [19], it is

reasonable to approximate a constant $\nu_p(t)$ equal to the instantaneous elastic value in the absence of conclusive contradictory data; such an approximation requires that the dilatational creep rate is equivalent to the uniaxial creep rate, and results in a simplification of Eq. (12) to

$$\overline{B}_p(s) = 3\left(1-2\nu_p\right)\overline{J}(s), \tag{13}$$

which may be directly inverted to the time-domain to find

$$B_p(t) = 3\left(1-2\nu_p\right)J_p(t), \tag{14}$$

where ν_p is the instantaneous elastic Poisson's ratio.

Combination of Eqs. (11) and (14) yields

$$\varepsilon(t) = 3\left(1-2\nu_p\right)\int_0^t \frac{\partial\sigma(t')}{\partial t'}J_p(t-t') + \frac{\partial P(t')}{\partial t'}\left(3\left(1-2\nu_p\right)J_p(t-t')-\frac{1}{K_s}\right)dt' \tag{15}$$

for the dilatational strain of a linear poroviscoelastic material.

For a solidifying linear poroviscoelastic material with intrinsic aging of the solidifying material, Eq. (15) becomes

$$\varepsilon(t) = 3\left(1-2\nu_p\right)\int_0^t \frac{\partial\sigma(t')}{\partial t'}J_p(t,t') + \frac{\partial P(t')}{\partial t'}\left(3\left(1-2\nu_p\right)J_p(t,t')-\frac{1}{K_s}\right)dt', \tag{16}$$

where $J_p(t,t')$ is defined by Eq. (10). Eq. (16) presents the proposed constitutive equation for predicting the volumetric free shrinkage of HCP when $\sigma(t)=0$; axial strain may be determined by dividing Eq. (16) by a factor of 3. The following subsections will detail the determination of the effective pressure that will be used in place of P in Eq. (16) to model desiccation shrinkage.

2.2. Driving forces and RVE

Chemical binding of evaporable water through hydration or moisture loss due to mass transport to the drying boundaries causes an initially saturated cementitious material (neglecting entrained or entrapped air) to desaturate resulting in the formation of vapor-filled spaces within the pore network and liquid menisci to retract from drying surfaces. After a small amount of desiccation, the liquid–gas interface will have a radius of curvature corresponding to the degree of liquid saturation and the corresponding *RH*. The high interfacial energy between water and the solid phases leads to adsorbed water films forming in areas where bulk capillary water does not exist. Therefore, at any point in time, a representative volume element (RVE) for modeling shrinkage of cementitious materials should consist of several phases:

1. liquid water in the pore network with dissolved gases and ions,
2. gas bubbles in the pore network consisting of water vapor and other gases,
3. solid, and
4. adsorbed film/interfaces in the pore network.

The RVE to be utilized in the derivation of the shrinkage model is shown in Fig. 1, where the sample is considered in equilibrium with and open to the surrounding gas (and thus vapor pressure).

2.2.1. Local liquid–gas equilibrium

Assumption of local liquid–gas equilibrium in the RVE allows the determination of the pore fluid pressure as a function of local *RH*. In the case of a pore fluid consisting of pure water, the Kelvin–Laplace equation describes the liquid–gas equilibrium. However, when

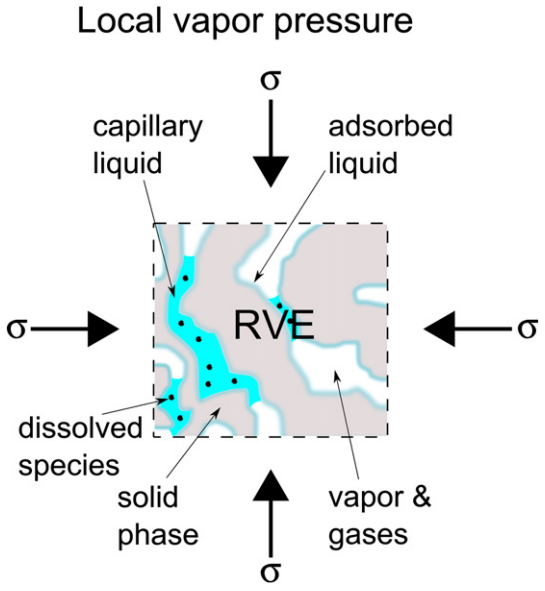

Fig. 1. Representative volume element (RVE) for desiccation shrinkage model. The RVE is assumed open (allowing mass transfer of water) and in full thermodynamic equilibrium with the local *RH*. σ is the externally applied volumetric stress.

dissolved species are present in the pore fluid (as in cementitious materials), the Kelvin–Laplace equation no longer describes equilibrium. In desiccating cementitious materials, the concentration of dissolved species is not expected to be constant with time; as moisture vacates the pore network, the concentration should increase up to some maximum concentration whence precipitation will occur. However, for high solubility species (e.g. K, Na) precipitation will only occur at very low saturation. The following derivation results in a modified Kelvin–Laplace equation that accounts for the effect of changing concentrations of dissolved species in the pore fluid during desiccation on the pore fluid pressure at a given *RH*. Such changes in the pore solution chemistry during drying have been noted in the literature [16] and used to partially explain the effect of shrinkage reducing admixtures on internal *RH* in cementitious materials [17,39].

Following [40], a Gibbs–Duhem relationship for the liquid and gas phases in the RVE may be expressed according to

$$\begin{aligned} dP_g &= s_g dT + n_g^v d\mu_g^v + n_g^{air} d\mu_g^{air} \\ dP_l &= s_l dT + n_l^w d\mu_l^w + n_l^{diss} d\mu_l^{diss}, \end{aligned} \tag{17}$$

where μ_g^v is the molar specific chemical potential of the water vapor, μ_g^{air} is the sum of the molar specific chemical potentials of each of the molecular species present in the gas (other than water vapor), μ_l^w is the molar specific chemical potential of the liquid water, and μ_l^{diss} is the molar specific chemical potential of the dissolved species. Likewise, n_g^v is the molar (volume) concentration of water vapor in the gas, n_g^{air} is the molar concentration for other molecules in the gas, n_l^w is the molar concentration of water in the liquid, and n_l^{diss} is the molar concentration of dissolved species in the liquid. The molar concentration of dissolved gases is assumed negligible, and the additional dissolved species in the pore fluid are assumed non-volatile such that they have negligible gaseous molar concentration. This means that the effect, for example, of dissolved CO_2 on μ_l^w is ignored in this model, but could be accounted for by including an additional term in Pitzer's equation as presented in the following derivation. The terms s_g and s_l are the volume specific entropies of the gas and liquid phases, respectively, while T is the temperature. As we are stipulating isothermal conditions, the entropic terms disappear. Additionally, if

we stipulate constant composition during a small change in equilibrium conditions we can write

$$\left(\frac{\partial \mu_l^w}{\partial P_l}\right) = v_l^w, \tag{18}$$

where $v_l^w = 1/n_l^w$ is the molar volume of liquid water. Assuming the gaseous mixture behaves in an ideal manner for a small change in equilibrium at constant temperature,

$$d\mu_g^v = \frac{RT}{P_g} dP_g. \tag{19}$$

For a change from one equilibrium state to another, the change in chemical potential of each species and its vapor must be equal. Therefore, $d\mu_l^w = d\mu_g^v$ such that for isothermal conditions

$$dP_l = \frac{RT}{v_l^w P_g} dP_g, \tag{20}$$

where Eqs. (18) and (19) have been used.

Approximating liquid water as incompressible, integrating Eq. (20) from a condition where $P_l = P_g^{v-0}$ to some other state results in

$$P_l - P_g^{v-0} = \frac{RT}{v_l^w} \ln\left(\frac{P_g^v}{P_g^{v-0}}\right), \tag{21}$$

where P_g^{v-0} is the vapor pressure over the liquid mixture when $P_g = P_l$ (i.e. over a flat surface of liquid mixture). Adding P_g^v to both sides of Eq. (21) we find that

$$P_c = \left(P_g^v - P_g^{v-0}\right) - \frac{RT}{v_l^w} \ln\left(\frac{P_g^v}{P_g^{v-0}}\right) \approx -\frac{RT}{v_l^w} \ln\left(\frac{P_g^v}{P_g^{v-0}}\right), \tag{22}$$

which reduces as shown since $|P_c| \gg |(P_g^v - P_g^{v-0})|$. For the vapor pressure over the flat surface of the liquid mixture we can write

$$P_g^{v-0} = P_g^{v-0^*} a_l^w, \tag{23}$$

where $P_g^{v-0^*}$ is the vapor pressure over a flat surface of pure water at temperature T (i.e. "saturation" vapor pressure) and a_l^w is the activity of the water component in the liquid phase[4]. Eq. (23) expresses how the water vapor pressure of an aqueous solution is suppressed by the presence of dissolved species. Combining Eqs. (22) and (23) results in

$$P_c = \frac{-RT}{v_l^w} \left[\ln\left(\frac{RH}{100}\right) - \ln a_l^w\right]. \tag{24}$$

where $RH = P_g^v / P_g^{v-0^*} \times 100$ ranges from 0–100%. As cementitious materials dry, it is expected that a_l^w will decrease due to the increasing concentrations of dissolved species in the pore fluid. Neglecting precipitation or dissolution during the drying process, a_l^w may be defined with a relatively high degree of accuracy over the full range of saturation using Pitzer's equations [41] according to

$$a_l^w = \exp\left[\frac{-\chi \sum_i n_l^i}{n_l^w}\right], \tag{25}$$

where n_l^i are the molar concentrations of the dissolved species, n_l^w (≈ 55.51 mol/L) is the molar concentration of water, and

$$\chi = 1 + \frac{2}{\sum_i n_l^i} \left[\frac{-AI^{3/2}}{1 + bI^{1/2}} + \sum_c \sum_a n_l^c n_l^a \left(B_{ca}^{\chi} + ZC_l^{\chi}\right) + \sum mt\right] \tag{26}$$

is the osmotic coefficient. The terms n_l^i refer to the molar concentrations of all dissolved species (which are a function of S), I is the ionic strength, A is the Debye–Hückel osmotic coefficient parameter, n_l^c and n_l^a are the molar concentrations of the cations and anions in solution, respectively, B_{ca}^{χ} and C_{ca}^{χ} are empirical cation–anion specific interaction parameters, and

$$Z = \sum_i n_l^i |z_i|, \tag{27}$$

where z_i are the charges associated with the ions in solution. The final term in Eq. (26) refers to the sum of the mixing terms that quantify the effect of interactions between multiple cations and anions.

At low concentrations of dissolved species the mixture may be treated as ideal and the water activity calculated according to Raoult's law as

$$a_l^w = \frac{n_l^w}{n_l^w + n_l^{diss}/S} = 1 - \frac{n_l^{diss}}{n_l^w S + n_l^{diss}}, \tag{28}$$

where $n_l^{diss} = \sum_i n_l^i (S = 1)$ is the total molar concentration of all dissolved species prior to drying (i.e. the total molar moles of dissolved species divided by the pore volume). Fig. 2 plots a_l^w determined through Eq. (25) utilizing B_{ca}^{χ} and C_{ca}^{χ} obtained from [41] and [42] assuming the following $n_l^i(S=1)$ in mmol/L [43]: Na^+: 332, K^+: 695, Ca^{2+}: 3, OH^-: 839, and SO_4^{2-}: 44. The mixing terms were neglected due to lack of available empirical coefficients in the literature, but this is not expected to introduce significant error since these terms are relatively small except at extremely low S. Fig. 2 also plots a_l^w determined through Eq. (28), and a comparison of the plot with that of Eq. (25) indicates that Raoult's law yields an accurate a_l^w (for the pore solution given) down to $S \approx 0.5$. Since the total concentration of dissolved species considered in Fig. 2 is $n_l^{diss} = 1.9$ mol/L, which is higher than one would find in most cementitious materials, one would

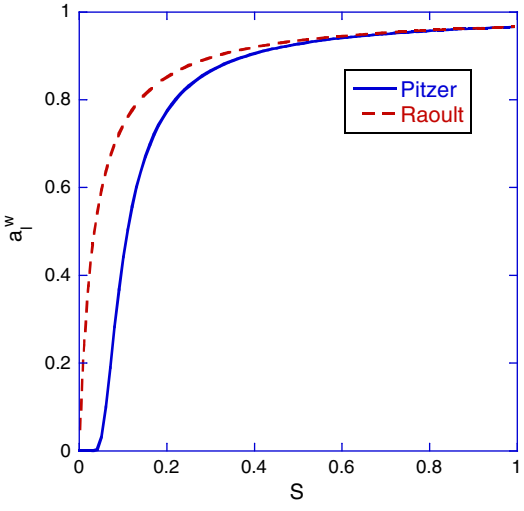

Fig. 2. Comparison of water activity calculations using Pitzer's equation (Eq. (25)) and Raoult's Law (Eq. (28)) for a pore solution of typical initial concentrations (from [43]) of dissolved species subjected to moisture loss (i.e. drying). For the system considered, Raoult's law is accurate until $S \approx 0.6$, but this may not be the case for all cementitious systems. As such, Pitzer's approach [41] should be considered most accurate over the full range of S.

[4] In this paper, the activity is defined by the reduction in vapor pressure of a solvent (in this case water) due solely to the presence of solutes. In some works, activity of the solvent is defined by the reduction in vapor pressure attributable to any sources.

expect Raoult's law to yield an accurate measure of a_l^w down to at least $S \approx 0.5$ in many cementitious materials. However, one should keep in mind that Pitzer's approach [41] yields the most accurate quantification of activity reduction of the full range of S. For most practical applications where concrete is exposed to ambient conditions, one can combine Eqs. (24) and (28) to obtain

$$P_c \approx \frac{-RT}{v_l^w}\left[\ln\left(\frac{RH}{100}\right) + \ln\left(1 + \frac{n_l^{diss}}{n_l^w S}\right)\right]. \tag{29}$$

During the desiccation process, n_l^{diss} may be approximated as constant, although chemical reactions, dissolution, precipitation, and adsorption make this unlikely in reality. For example, it is known that alkalis are continuously released on dissolution of clinker, but also continuously bound with C–S–H [44]. However, with the $n_l^{diss} =$ constant approximation, if the constitutive function for $S(RH)$ is known, then Eq. (29) provides an expression for calculating P_c strictly as a function of the local RH, T, and initial pore solution dissolved species concentration. Eq. (29) describes capillary pressure development in the RVE as local RH is reduced while accounting for the effect of increasing concentration of dissolved species in the pore fluid as desiccation progresses. Note that if $n_l^{diss} = 0$, then Eq. (29) reduces to the classical Kelvin–Laplace relationship. Furthermore, by setting $S = 1$ and $P_c = 0$ in Eq. (29), the equilibrium RH of the pore solution with a flat liquid/gas interface may be calculated. As an example, for a pore solution ionic concentration of 1.91 mol/L [43], the equilibrium RH at 20 ° C is calculated as 96.7%.

When modeling desiccation shrinkage of cementitious materials, if the sorption isotherm is experimentally determined, the effect of changing concentration of dissolved species on the surface tension of the pore fluid and the resulting impact on S is inherently accounted for. Therefore, neglecting the effect of increasing pore solution concentrations when modeling desiccation shrinkage will always be to over predict the P_c in the pore network, resulting in an over-prediction of shrinkage.

It should be noted that the magnitude of the effect of neglecting dissolved species on the calculated P_c (and thus shrinkage) is dependent on the sorption isotherm. For example, if a material has a substantial volume fraction of large pores, then the sorption isotherm will be quite steep at high RH; the result will be a rapid increase in the concentration of dissolved species during initial desiccation and a more rapid deviation in the actual P_c from that of pure water. Therefore, P_c in early age concrete (which has a large volume fraction of larger pores) would likely be more strongly impacted by the presence of dissolved species in the pore fluid than older concrete.

A final comment on the derivation of Eq. (29) is that acknowledgment of the presence of a meniscus was not necessary for the derivation. The implication is that Eq. (29) is valid (as a thermodynamic equilibrium condition) over the full range of RH, even though menisci are only stable above some threshold RH (suggested to be about 70% RH by Weiss et al. for a plain cement system [17]). Therefore, P_c is a thermodynamic state variable [45] over the full range of RH, which implies that capillary pressure may be quantified even in the absence of a defined meniscus; this suggestion conflicts with suggestions in the literature that shrinkage stresses are reduced in systems once the meniscus breaks down. However, the derivation of P_c *does* depend on the assumption of a continuum, which breaks down when considering pore diameters of the same length scale as the molecular diameter of the species in the pore fluid.

2.2.2. Local liquid–solid–vapor-interface physicochemical equilibrium

The preceding section utilizes the equilibrium of the liquid and gas phases to derive a relationship between P_c and the local RH. However, Coussy et al. [4] have shown that there is an additional pressure applied within the pore network induced by the presence of interfaces. This additional pressure is induced principally due to the mechanism often referred to as "changes in solid surface free energy." When adsorbed water films change thickness as the local vapor pressure is reduced, the effective surface free energy of the coated solid phases increases, leading to compression of the material (in order to reduce the exposed surface area and minimize the energy). As will be shown, the relative importance of changes in solid surface free energy at a particular RH is dependent on the desorption isotherm for the material (which describes the fraction of empty porosity at a given RH); for a typical concrete, the effect is only significant at about $S \leq 0.6$. Coussy et al. [4] showed that the additional pressure in the desiccating pore network induced by interfaces is

$$U(S) = \int_S^1 P_c(S')dS', \tag{30}$$

where S' is the dummy saturation variable of integration. Thus, the *effective* pressure in the pore network (accounting for both capillary pressure and interface induced pressure) is

$$\pi = P_{avg} - U, \tag{31}$$

where the negative sign on U reflects the tensile nature of the pressure within the surface layer (causing compression of the solid phase). Since U is a function of P_c, it will be affected by inclusion or neglection of the dissolved species in the pore fluid in the same manner as with P_c.

In order to predict the volumetric strain of cementitious materials accounting for capillary pressure as well as the additional interface induced pressure, it is necessary to substitute π into Eq. (16) for P to obtain

$$\varepsilon(t) = 3(1-2\nu)\int_0^t \frac{\partial \sigma(t')}{\partial t'} J_p(t,t') + \frac{\partial \pi(t')}{\partial t'}\left(3(1-2\nu)J_p(t,t') - \frac{1}{K_s}\right)dt', \tag{32}$$

while the axial strain is determined by dividing Eq. (32) by a factor of 3. Free desiccation shrinkage strain is obtained in the absence of externally applied pressure (i.e. when $\sigma(t) = 0$).

3. Experimental

Experimental evaluation of the modeling previously discussed was achieved by measuring drying shrinkage of HCP specimens subjected to a single step-wise reduction in RH from ≈100% to 50% in a controlled environmental chamber. In order to predict the measured shrinkage according to the model described in the previous sections, aging viscoelastic constitutive properties and desorption constitutive properties were also experimentally measured. Formulation of the desorption isotherms required measuring mass loss during multiple small step-wise reductions in ambient RH along with the evolution of the porosity with age. For each experiment, duplicate specimens were tested and the average value used. Minimal difference was observed when comparing the results of each duplicate specimen.

An ASTM Type I cement was used for the test specimens and the fresh cement paste was mixed in accordance to ASTM C305-06. The HCPs tested were 0.4 and 0.5 w/c, and were 3 and 7 days old at the beginning of each test. Both mass loss and drying shrinkage specimens consisted of thin, plate-like strips drying from all sides (the drying is essentially 1-D symmetric drying because of the plate-like geometry). The HCP strips with dimensions of 45 mm wide, 2 mm thick, and 200 mm long were made by casting fresh cement paste on an acrylic sheet with individual specimens separated by 2 mm thick acrylic strips. Exact dimensions of each specimen were measured with

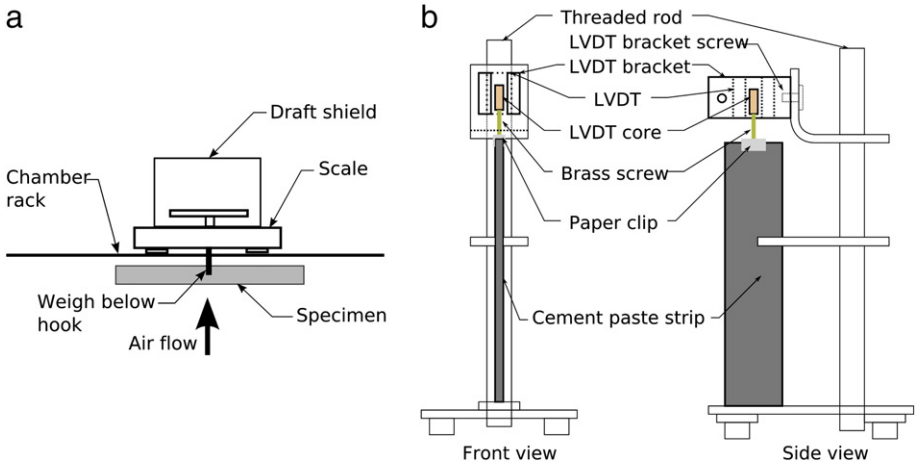

Fig. 3. Mass loss measurement apparatus and drying shrinkage measurement apparatus.

calipers to account for any variability in the mold dimensions. Specimens were made thin in order to reduce time necessary for the equilibration of water mass loss during the drying process. The mold containing fresh cement paste with the finished surface was placed in a 100% *RH* (non-condensing) environment for curing. HCP strips were demolded after 24 h and then placed in a vacuum-sealed container filled with water. Shrinkage of the materials was measured in a separate test utilizing identically fabricated (and cured) specimens as in the mass loss tests. The evolution of porosity with age for each material was determined via the oven drying method (see, e.g. [6,46]).

Specimens for measuring elastic and viscoelastic properties were made by mixing cement pastes according to ASTM C305-06. Specimens with *w/c* of 0.4 and 0.5 were cast into 102 mm diameter by 200 mm height plastic cylinder molds. The specimens were demolded at 24 h and stored in a moisture room until a few hours prior to testing.

3.1. Measurement of shrinkage and mass loss

Specimens used for measuring shrinkage and mass loss of HCP were maintained in an environmental chamber capable of rapidly changing and maintaining constant *RH* (±3%) and temperature (±0.5 °C). Temperature level within the chamber was fixed at 23 °C throughout the testing program. Specimens used to measure mass loss were fastened with a clip and mounted under a precision scale that was placed on a rack near the middle of the chamber. Fig. 3a is an illustration of the experimental setup for mass loss measurement inside the chamber. For determination of the desorption isotherms, chamber *RH* steps were performed in about 10% increments, with the initial chamber *RH* set between 100 and 95%. The chamber *RH* reached a low of 25% at the end of each test. The duration of each step for mass loss measurements was manually controlled, and varied between 5 and 24 h depending on the drying rate at each step; i.e. some of the higher *RH* steps required shorter time for sufficient mass equilibration than the lower *RH* steps. Mass loss was measured by precision scales interfaced with an RS232 port for automated PC data acquisition. Typical mass loss data for multiple step-wise reductions in chamber *RH* are shown in Fig. 4.

Equilibrium mass loss data can be readily converted to saturation (*S*) in order to construct desorption isotherms when the porosity of the material and the dimensions of the test specimens are known [55]. As seen in Fig. 4, the specimen mass was not fully equilibrated at the end of each step in chamber *RH*, particularly when the chamber was at lower *RH*. In such cases, the equilibrium mass for the step in question was extrapolated by fitting an exponential decay function to the measured mass loss data. Based on the extrapolated equilibrium mass at each *RH* step, desorption isotherms were constructed for each material at each testing age, and are shown in Fig. 5. As expected, the desorption isotherms shift upward as *w/c* is decreased and age is

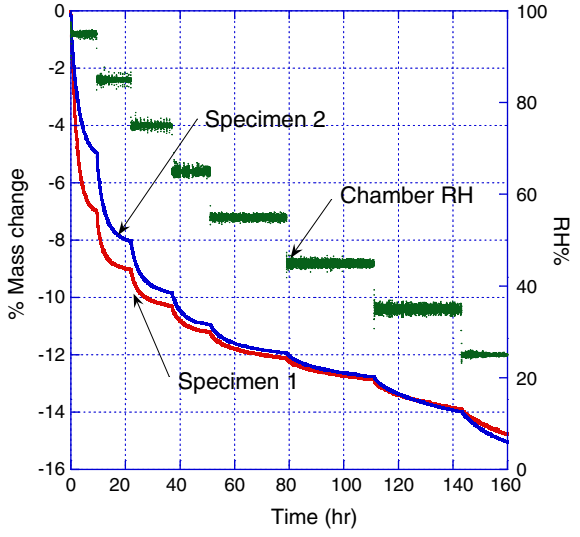

Fig. 4. Example measured mass loss due to drying during multiple step-wise reductions in chamber *RH*.

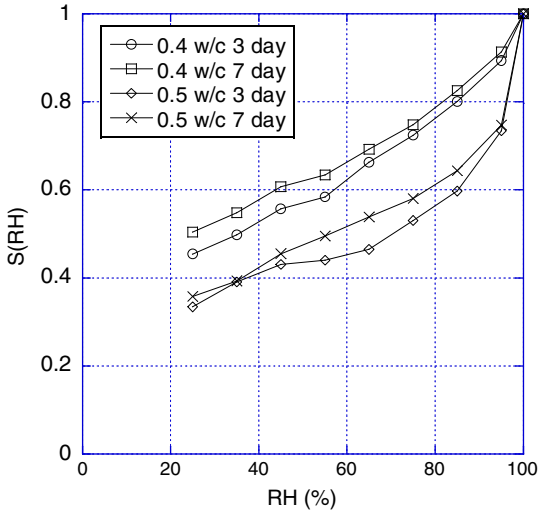

Fig. 5. Desorption isotherms for each material and age of interest.

Table 1
Viscoelastic and elastic parameters used in modeling spring constants (E_i) given in GPa, retardation times (τ_i) given in days.

	0.4 *w/c* 3 days	0.4 *w/c* 7 days	0.5 *w/c* 3 days	0.5 *w/c* 7 days
E_0	17.1	21.5	9.0	12.2
E_1	15.6	18.5	15.8	22.7
E_2	2.4	6.5	2.0	2.9
τ_1	1.7	1.1	0.2	0.3
τ_2	10	10	10	10
ν_p	0.28	0.28	0.32	0.32

increased. Upward shifts in the desorption isotherm imply a smaller average pore size.

To measure axial shrinkage, simple frames were constructed to hold the specimens and Linear Variable Differential Transformers (LVDTs) were used to measure axial displacement, with a gage length (specimen length) of about 203 mm. Fig. 3b. illustrates the experimental setup for axial shrinkage measurement. The shrinkage specimens were subjected to a single step-wise reduction in chamber *RH* from ≈100% to 50%. Mass loss was also measured for the single step-wise reduction in chamber *RH* in order to determine $S(t)$ for the drying shrinkage specimens using the desorption isotherms.

To prevent carbonation during the shrinkage and mass loss experiments, reagent grade lithium hydroxide monohydrate crystals ($LiOH–H_2O$) [47,48] were placed in the chamber in order to absorb carbon dioxide from the air in the chamber prior to the starting of the experiments. After the shrinkage and mass loss testing completed, the strips were tested for carbonation by spraying a 2% phenolphthalein solution on the specimens. No carbonation was indicated by the phenolphthalein tests.

3.2. Measurement of Young's modulus and uniaxial viscoelastic compliance

Elastic and viscoelastic material properties control how a given material will respond to internal pore stresses (or stresses in general) as in the case of desiccation shrinkage. The instantaneous elastic Young's modulus (E_0) of each material was measured by unconfined compression according to ASTM C469 by recording axial displacement and applied force, with the results shown in Table 1. The Young's modulus was measured for each material at ages of 3 and 7 days, and the solidification aging function $v(t)$ was determined by normalizing the Young's modulus data to the value at the age of the start of the shrinkage tests, then fitting to

$$v(t) = \frac{v_1 v_2 t^{1-v_3}}{1 + v_2 t^{1-v_3}}, \tag{33}$$

where v_1, v_2, and v_3 are fitting parameters. The form of the aging function shown in Eq. (33) was chosen since it allows analytical integration of Eq. (10). The fit parameters for each material and each testing age are shown in Table 2. The use of evolution of Young's modulus with age to define the aging function for the solidification theory is supported by the fact that Young's modulus is known to scale linearly with degree of hydration [49].

Viscoelastic properties were determined by a constant load creep test according to ASTM C512, except that embedment strain gages were cast directly into the cylinders for measuring axial strain. The cylinders were demolded after 24 h and wrapped with aluminum foil backed adhesive tape to prevent drying from occurring[5]. High strength capping compound in accordance with ASTM C-617 was used to ensure centric loading of specimens. To prevent temperature effects, both the elastic and creep tests were conducted in a temperature controlled room (maintained at 23 °C). The use of embedded strain gages allowed the collection of strain data throughout the creep tests, which were started at ages of 3 and 7 days for each material in order to determine viscoelastic properties relevant to the shrinkage tests started at the same ages. A load cell was placed in the creep loading frame to record load loss during each test. As the specimens deformed, applied load relaxed due to the change of the compressed length of the springs. By obtaining a load curve with respect to time instead of assuming a constant load, the viscoelastic compliance was more accurately calculated. To avoid damaging the specimens during the creep tests, the uniaxial stresses applied to the specimens were between 1.9 and 3.5 MPa, which was expected to be less than 10% of the compressive strength of the materials. Creep strain history for each of the materials tested and their respective initial applied compressive stress are shown in Fig. 6.

Table 2
Curve fitting parameters for the solidification aging function shown in Eq. (33).

	0.4 *w/c* 3 days	0.4 *w/c* 7 days	0.5 *w/c* 3 days	0.5 *w/c* 7 days
v_1	1.7013	1.3599	1.1814	1.4010
v_2	0.5743	0.5793	0.4849	0.4849
v_3	0.1842	0.1816	0.1612	0.1612

Since no external drying occurred during the creep tests, it was assumed that hydration was progressing during the tests and that increased solidification was the only source of aging in the tests. Additionally, as the *w/c* for each material was reasonably high, it was assumed that shrinkage due to self-desiccation during the creep tests was negligible. Therefore, the measured creep data was fit to the constitutive equation for the solidification theory, expressed Eqs. (4) and (5). The actual measured stress history for each creep test was included in the fitting such that any load loss during the test was accounted for. The uniaxial viscoelastic compliance of the solidifying material, $J_s(t)$, was expressed according to a Prony series as

$$J_s(t) = 1/E_0 \sum_{i=1}^{n} \frac{1}{E_i}\left(1 - e^{(-t/\tau_i)}\right), \tag{34}$$

where E_i and τ_i denote spring constants and retardation times for each Kelvin unit i, respectively. The fitted E_i and τ_i for each material at each age are shown in Table 1. The Poisson's ratios (see Table 1), which

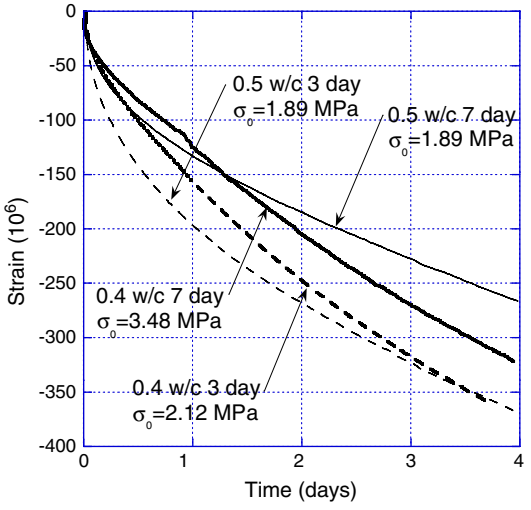

Fig. 6. Measured strain history from uniaxial creep tests with initial applied load indicated for each test.

[5] Viscoelastic properties of sealed specimens were measured rather than of drying specimens. Desiccation shrinkage is the mechanical response to stresses applied within the pore network. It has been hypothesized that the possible mechanisms for drying creep (e.g. stress-induced shrinkage, microcracking, etc.) are not active when the stresses are applied strictly within the pore network.

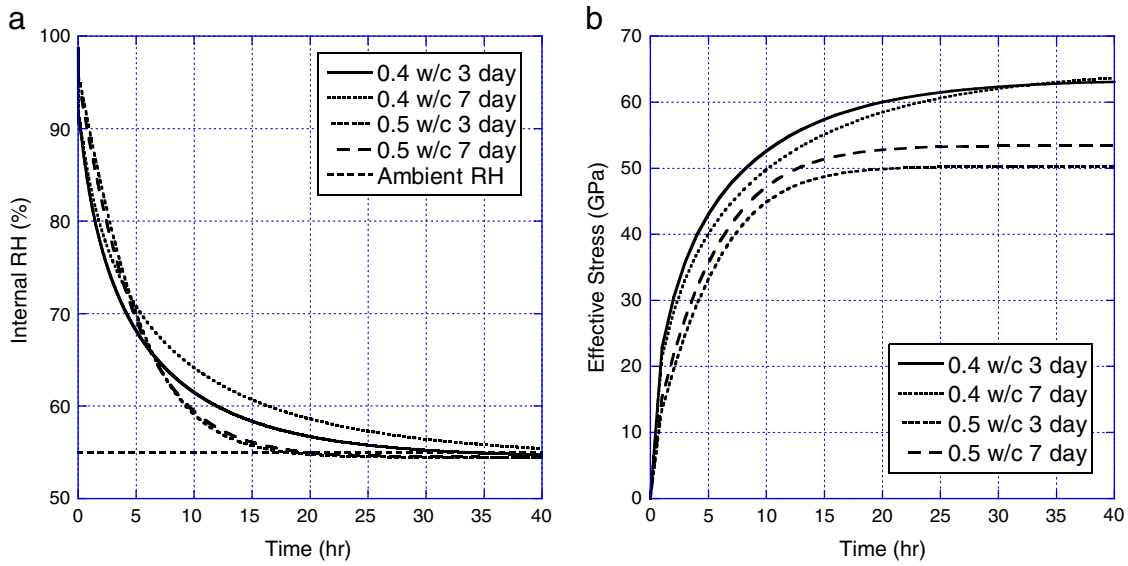

Fig. 7. Prediction of spatially averaged internal *RH* and effective pressure histories for each material subjected to a single step-wise reduction in chamber *RH* at ages of 3 and 7 days.

were assumed constant with time, were approximated based on literature values given in [49–51].

4. Prediction of stress history

Once the elastic and viscoelastic properties of a material are known, shrinkage of the material as a function of through-thickness position x and time elapsed since start of drying t can be modeled with a known effective pore pressure history. The effective pore pressure history is based on $RH(x,t)$ and $S(x,t)$ through Eq. (31). Since we are assuming *linear* viscoelastic behavior, the spatially averaged shrinkage strain obtained using the spatially averaged $\langle RH(x,t)\rangle$ and $\langle S(x,t)\rangle$ should be identical to the average shrinkage strain obtained by spatially averaging the shrinkage strain field for the specimen. $\langle S(x,t)\rangle$ for each shrinkage test is easily determined from the measured mass loss during the shrinkage test. With $\langle S(x,t)\rangle$ known, $\langle RH(x,t)\rangle$ for each test was determined using the desorption isotherms for the particular material and age. Fig. 7a shows the spatially averaged modeled internal $\langle RH(x,t)\rangle$ for each shrinkage test. Note that the average internal $\langle RH(x,t)\rangle$ decays to a value below the chamber *RH* due to the presence of dissolved species in the pore solution. The effect of dissolved species in the pore fluid on *RH*, *S*, and P_c was accounted for by using Eq. (29) by approximating n_i^{diss} for each material at each age according to Taylor's method [52,53] using the oxide composition of the low-alkali cement provided by the manufacturer. It was assumed that hydroxide ions were present in the solution to balance the charge of the alkali cations predicted by Taylor's method, which yielded total n_i^{diss} ranging from 280–366 mmol/L, depending on the w/c ratio and age.

Once $\langle P_c(x,t)\rangle$ and $\langle S(x,t)\rangle$ were determined for each material at each age, the spatially averaged effective pressure history of each specimen ($\langle \pi(x,t)\rangle$) was determined according to Eq. (31). Fig. 7b shows the spatially averaged predicted effective pressure history ($\langle \pi(x,t)\rangle$) for each shrinkage specimen.

5. Comparison of measured and modeled shrinkage

Shrinkage measurements for all of the materials tested were an average between two specimens that showed negligible deviation from each other. To provide insight into the desiccation shrinkage phenomenon, shrinkage predictions were performed according to several material models:

- solidifying poroelastic,
- poroviscoelastic,
- solidifying poroviscoelastic, and
- solidifying poroviscoelastic with intrinsic aging of J_s through the time-shift approach.

All four predictions were made using Eq. (32) (divided by 3 for axial strain), with each of the first three cases listed above determined as limit cases of the general model (i.e. the model for the fourth case). The solidifying poroelastic model was determined by letting $\tau_i \to \infty$ such that the second term in Eq. (5) goes to zero. The non-aging poroviscoelastic prediction was obtained by setting $v(t) = 1$ in Eq. (5) and $\mu = 0$ in Eq. (6). The solidifying poroviscoelastic prediction was obtained by setting $\mu = 0$ in Eq. (6).

Fig. 8 compares the predicted drying shrinkage according to the solidifying poroelastic, poroviscoelastic, and solidifying poroviscoelastic models to measured drying shrinkage data for each material exposed to a step-wise reduction in boundary *RH* from ≈100% to 55% at ages of 3 and 7 days. The first important feature of Fig. 8 to note is that shrinkage prediction for the solidifying poroelastic material asymptotes by about 1 day, while the measured shrinkage continues to increase steadily throughout the test. The implication of this result is that, as suggested in previous research [16,24], there is a viscoelastic component to shrinkage strain. Another feature to note in Fig. 8 is that both the poroviscoelastic and solidifying[6] poroviscoelastic predictions dramatically over predict the measured shrinkage. In general, there was about 20–30% additional shrinkage measured after the point at which mass loss, and thus changes in internal pore pressure, ceased. However, in the uniaxial creep tests there was at least a 100% increase in strain (versus elastic strain) after just 4 days under load due to creep. This corresponds to a relative decrease of about 400% in viscoelastic compliance from uniaxial loading to drying shrinkage, which clearly indicates that the viscoelastic properties under the two different types of loading (sealed uniaxial creep versus free shrinkage due to desiccation) are quite different. The reasons for differences in viscoelastic behavior between the two types of experiments are

[6] We acknowledge that any increased solidification during the drying shrinkage test is unlikely since the internal *RH* decays quite rapidly to a level not conducive to continued hydration. However, one might note in Fig. 8 that the solidification effect is minimal anyhow. We include the solidifying poroviscoelastic prediction to illustrate the minimal effect of solidification on the shrinkage prediction.

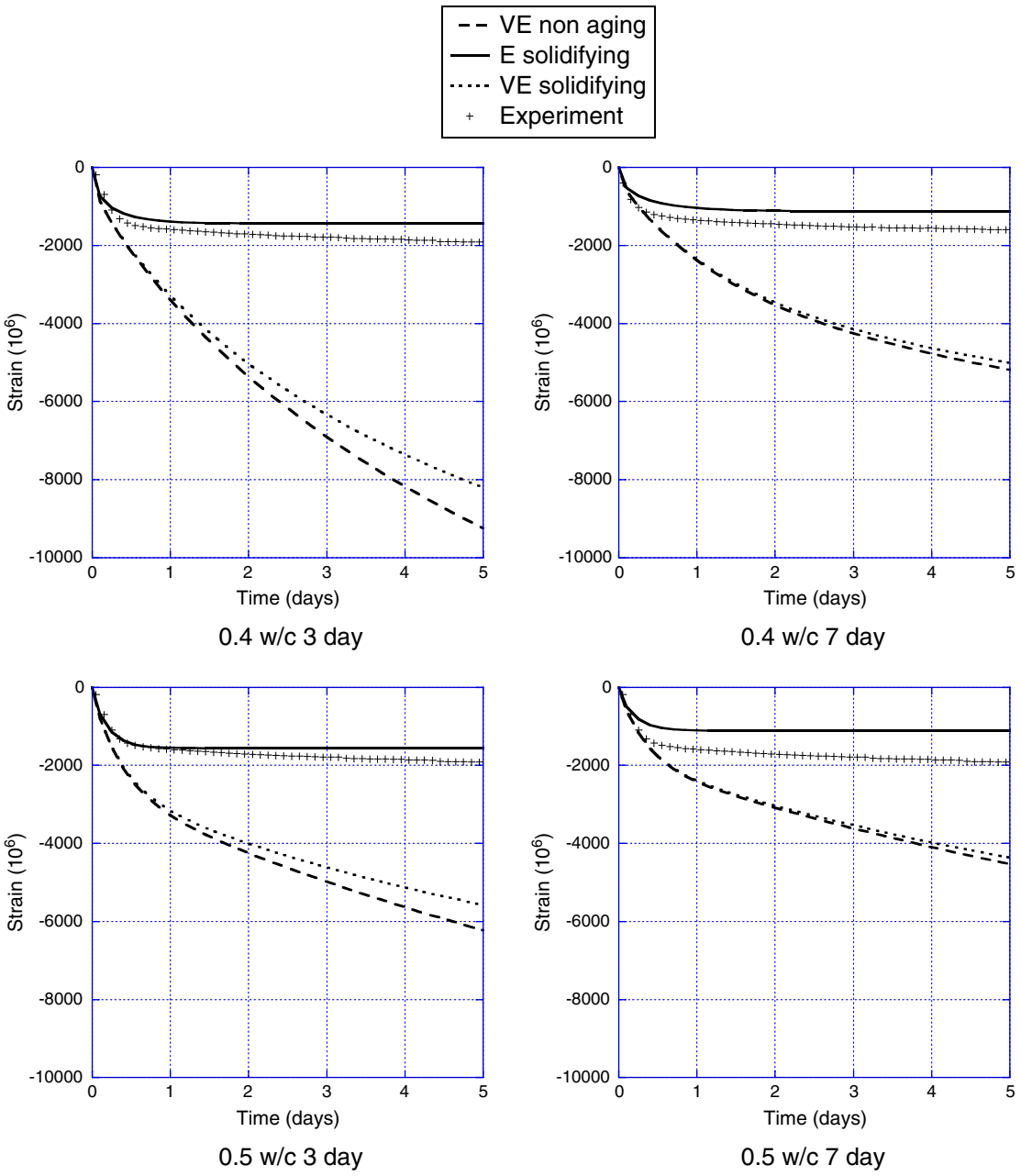

Fig. 8. Solidifying poroelastic ('E solidifying'), poroviscoelastic ('VE non-aging'), and solidifying poroviscoelastic ('VE solidifying') shrinkage model predictions in comparison to measured drying shrinkage. Drying was initiated with a step-wise reduction in chamber *RH* from ≈100% to 50% at the ages indicated.

postulated to be either of the following explanations, or a combination of the two explanations:

- aging effects are much greater when HCP is subjected to drying. Thomas et al. suggested that drying induces additional aging due to the compaction of C–S–H from the pore pressure [27], while others have suggested that drying increases polymerization of C–S–H [28], and/or
- the viscoelastic bulk modulus $K_p(t)$ relaxes more slowly than the viscoelastic Young's modulus $E_p(t)$. Previous research has shown that the uniaxial and bulk viscoelastic responses are different. There is evidence that using uniaxial viscoelastic compliance to predict bulk viscoelastic compliance might lead to a substantial over-prediction in relaxation rates [19], which could help explain the overprediction of shrinkage in this work. Having different time functions for $K_p(t)$ and $E_p(t)$ indicates an increasing viscoelastic Poission's ratio, which violates the assumption of a constant Poisson's ratio made in the model predictions. Different aging functions (either for the solidification function, intrinsic aging function, or both) for dilatational and deviatoric moduli would likewise explain the discrepancy. Uniaxial stress is 2/3 deviatoric and 1/3 dilatational.

If the difference in the shrinkage predicted with the solidifying viscoelastic model and the measured shrinkage is explainable by increased aging of the solidifying material in the drying problem, then the time-shift approach discussed in Part I could be used to account for the extra aging. Grasley and Lange [20] suggested that for young, sealed HCP with a *w/c* of 0.41, the aging function shown in Eq. (6) with $\mu = -0.7$ was sufficient to explain additional aging beyond that produced by solidification effects. Fig. 9 compares the measured drying shrinkage to the shrinkage predicted using the solidifying

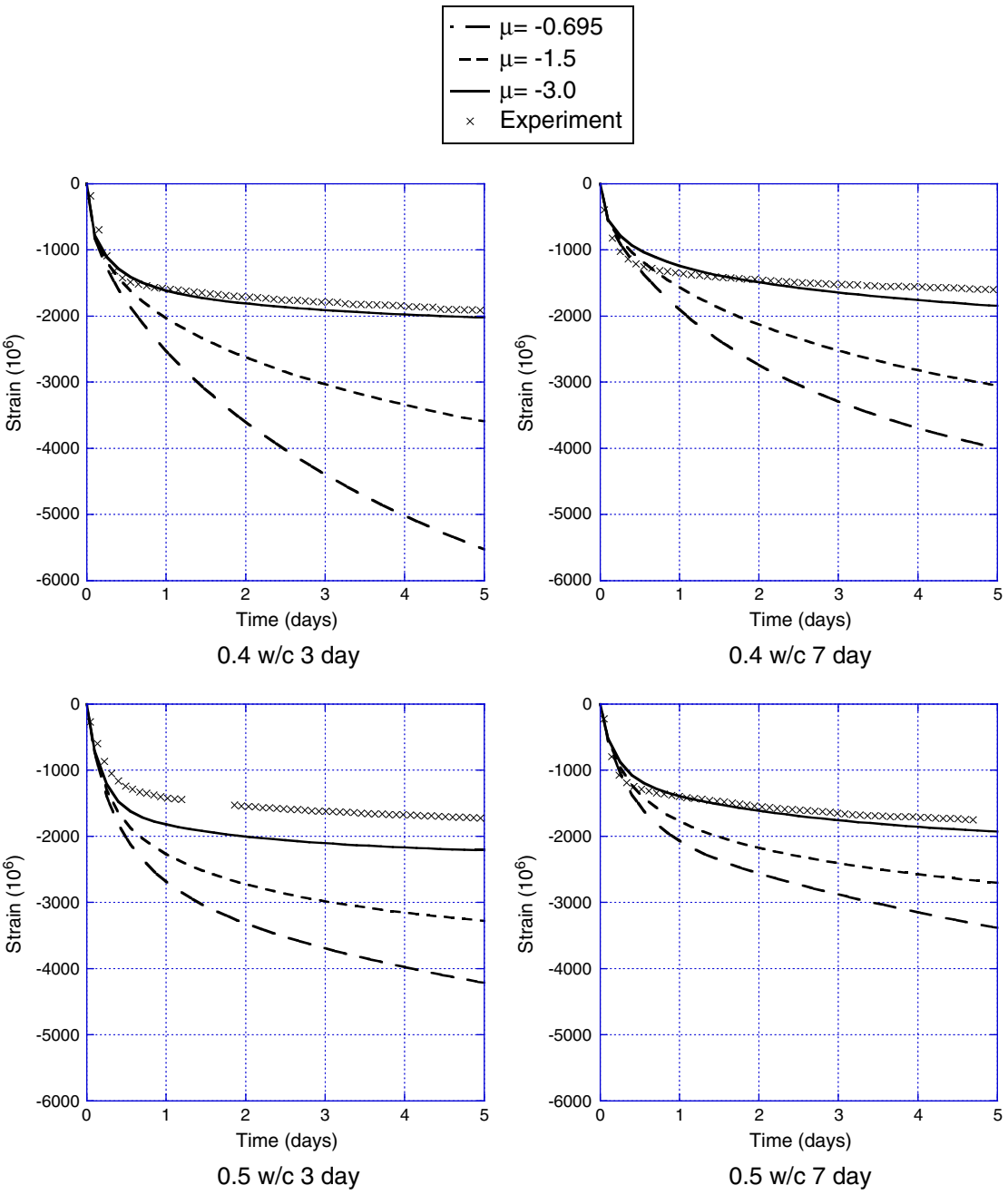

Fig. 9. Shrinkage predictions using the solidifying poroviscoelastic model with intrinsic aging of the solidifying C–S–H gel modeled using the time-shift approach.

viscoelastic model with intrinsic aging of the gel accounted for with the time-shift approach. When $\mu = -0.7$ is used, the model still significantly over predicts the measured shrinkage. It is not until μ is reduced to -3 that the shrinkage predictions approach the measured data, although based on the proposed effect of drying on the intrinsic aging of C–S–H, this is not an unexpected result. The internal *RH* of the sealed 0.41 w/c specimens considered by Grasley and Lange remained significantly higher than the internal *RH* of the specimens considered in this research.

Note that the difference between the poroviscoelastic and solidifying poroviscoelastic predictions shown in Fig. 8 is minimal, whereas the effect of the time-shift on the shrinkage prediction is quite substantial. Therefore, one can presume that in the case of drying shrinkage, intrinsic aging of the C–S–H gel is likely a first-order effect, while solidification is a less important, second-order effect — at least for the materials and age of initiation of drying considered in this work. One might also note that the solidifying poroelastic model yields a reasonable prediction of shrinkage — in fact, a better prediction than the poroviscoelastic or solidifying poroviscoelastic models. However, because of the history effect inherent to viscoelastic materials, one should not always expect the elastic prediction to be adequate for drying histories or materials different than those considered in this research.

The suggestion that substantial aging of the viscoelastic properties occurs during drying has potential implications on our understanding of drying creep (i.e. the Pickett effect [54]). Based on the results presented here, the drying creep effect could be induced by the applied external load, rather than by the drying; that is, the application of an externally applied load may influence the aging that normally occurs during drying in the absence of externally applied loads. For example, if drying-induced aging is caused by compaction of C–S–H colloidal particles, perhaps the application of an

external load retards the compaction process through the presence of introduced microscale shear stresses. Therefore, if a material under combined drying and external load ages less than a material that is not simultaneously under both external load and drying, superposition of the separate responses to drying and load will not equal the combined response. In light of the findings in this paper, the link between the drying creep effect and aging associated with drying deserves further investigation.

6. Conclusions

A new model has been developed for cementitious materials for predicting autogenous shrinkage, drying shrinkage, or a combination of the two. The new model is based on aging poroviscoelasticity, where the aging is accounted for through the use of the solidification theory in combination with the time-shift approach. In addition, the modeling approach accounts for the effect of changing concentrations of dissolved species in the pore fluid on desiccation shrinkage through changes in the effective pore pressure. The proposed model was evaluated by comparison of predicted drying shrinkage to measured drying shrinkage for two different *w/c* with drying initiated at two different ages. The model predictions presented include solidifying poroelastic, poroviscoelastic, solidifying poroviscoelastic, and solidifying poroviscoelastic with intrinsic aging of the solidifying C–S–H gel accounted for through the time-shift approach. Comparison of the various model predictions with the measured shrinkage data indicates the following:

- elastic predictions under predict the measured shrinkage, indicating a viscoelastic component to desiccation shrinkage,
- non-aging viscoelastic models and solidifying viscoelastic models significantly over predict the measured drying shrinkage, indicating that either additional aging is present when HCP is drying or that dilatational creep/relaxation of the porous body proceeds more slowly than uniaxial creep/relaxation, and
- the addition of intrinsic aging of the C–S–H using the time-shift approach in conjunction with the solidifying poroviscoelastic model greatly improves the drying shrinkage prediction. In fact, the measured drying shrinkage histories are well-predicted by the model, indicating that intrinsic aging of the C–S–H induced by drying may be substantial.

Acknowledgments

This work was supported by the Texas Engineering Experiment Station and the Texas Transportation Institute. The authors thank the anonymous reviewer who provided several insightful comments that greatly improved the final manuscript.

References

[1] S. Mindess, J.F. Young, D. Darwin, Concrete, 2nd ed.Prentice Hall, Inc., Upper Saddle River, NJ, 2002.
[2] T.C. Powers, Thermodynamics of volume change and creep, Mater. Struct. 1 (6) (1968) 487–507.
[3] Z.C. Grasley, D.A. Lange, M.D. D'Ambrosia, Drying stresses and internal relative humidity in concrete, in: J. Skalny (Ed.), Materials Science of Concrete, vii, American Ceramic Society, 2005, pp. 265–305.
[4] O. Coussy, P. Dangla, T. Lassabatere, V. Baroghel-Bouny, The equivalent pore pressure and the swelling and shrinkage of cement-based materials, Mater. Struct. 37 (265) (2004) 15–20.
[5] O. Coussy, P.J.M. Monteiro, Poroelastic model for concrete exposed to freezing temperatures, Cem. Concr. Res. 38 (1) (2008) 40–48.
[6] Z.C. Grasley, G.W. Scherer, D.A. Lange, J.J. Valenza, Dynamic pressurization method for measuring permeability and modulus: Ii. Cementitious materials, Mater. Struct. 40 (7) (2007) 711–721.
[7] G.W. Scherer, Characterization of saturated porous bodies, Mater. Struct. 37 (265) (2004) 21–30.
[8] G.W. Scherer, Dynamic pressurization method for measuring permeability and modulus: I. Theory, Mater. Struct. (2006).
[9] F.-J. Ulm, G. Constantinides, F.H. Heukamp, Is concrete a poromechanics material? — a multiscale investigation of poroelastic properties, Mater. Struct. 37 (265) (2004) 43–58.
[10] D.P. Bentz, E.J. Garboczi, D.A. Quenard, Modelling drying shrinkage in reconstructed porous materials: application to porous vycor glass, Modell. Simul. Mater. Sci. Eng. 6 (3) (1998) 211–236.
[11] J.K. Mackenzie, The elastic constants of a solid containing spherical holes, Proc. Phys. Soc. B 63 (1950) 2–11.
[12] O. Coussy, Poromechanics, John Wiley & Sons Ltd, West Sussex, England, 2004.
[13] A.W. Bishop, The principle of effective stress, Teknisk Ukeblad 39 (1959) 859–863.
[14] P. Lura, Autogenous Deformation and Internal Curing of Concrete, Delft University, Delft, The Netherlands, 2003.
[15] P. Lura, Y.E. Guang, K. van Bruegel, Effect of cement type on autoegenous deformation of cement-based materials, ACI SP 220-4 (2004) 57–68.
[16] P. Lura, O.M. Jensen, K. van Breugel, Autogenous shrinkage in high-performance cement paste: an evaluation of basic mechanisms, Cem. Concr. Res. 33 (2) (2003) 223–232.
[17] J. Weiss, P. Lura, F. Rajabipour, G. Sant, Performance of shrinkage-reducing admixtures at different humidities and at early ages, ACI Mater. J. 105 (5) (2008) 478.
[18] T. Rougelot, F. Skoczylas, N. Burlion, Water desorption and shrinkage in mortars and cement pastes: experimental study and poromechanical model, Cem. Concr. Res. 39 (1) (2009) 36–44.
[19] Z.C. Grasley, D.A. Lange, The viscoelastic response of cement paste to three-dimensional loading, Mech. Time Depend. Mater. 11 (1) (2007) 27–46.
[20] Z.C. Grasley, D.A. Lange, Constitutive modeling of the aging viscoelastic properties of portland cement paste, Mech. Time Depend. Mater. 11 (3–4) (2007) 175–198.
[21] W. Vichit-Vadakan, G.W. Scherer, Measuring permeability and stress relaxation of young cement paste by beam bending, Cem. Concr. Res. 33 (12) (2003) 1925–1932.
[22] H.M. Jennings, Colloid model of c–s–h and implications to the problem of creep and shrinkage, Mater. Struct. 37 (265) (2004) 59–70.
[23] B.T. Tamtsia, J.J. Beaudoin, Basic creep of hardened cement paste. A re-examination of the role of water, Cem. Concr. Res. 30 (9) (2000) 1465–1475.
[24] Z.C. Grasley, Measuring and Modeling the Time-dependent Response of Cementitious Materials to Internal Stresses, Ph.D, University of Illinois at Urbana-Champaign, Urbana, IL, 2006.
[25] Z. Bažant, Viscoelasticity of solidifying porous material — concrete, J. Eng. Mech. 103 (EM6) (1977) 1049–1067.
[26] I. Carol, Z.P. Bažant, Viscoelasticity with aging caused by solidification of nonaging constituent, J. Eng. Mech. 119 (11) (1993) 2252–2259.
[27] J.J. Thomas, A.J. Allen, H.M. Jennings, Structural changes to the calcium–silicate–hydrate gel phase of hydrated cement with age, drying, and resaturation, J. Am. Ceram. Soc. 91 (10) (2008) 3362–3369.
[28] A. Bentur, N.B. Milestone, J.F. Young, Creep and drying shrinkage of calcium silicate pastes. Ii: induced microstructural and chemical changes, Cem. Concr. Res. 8 (1978) 721–732.
[29] F. Benboudjema, F. Meftah, J.M. Torrenti, A viscoelastic approach for the assessment of the drying shrinkage behaviour of cementitious materials, Mater. Struct. 40 (2) (2007) 163–174.
[30] C. Hua, P. Acker, A. Ehrlacher, Analyses and models of the autogenous shrinkage of hardening cement paste: I. Modelling at macroscopic scale, Cem. Concr. Res. 25 (7) (1995) 1457–1468.
[31] M.A. Biot, Theory of elasticity and consolidation for porous anisotropic solid, J. Appl. Phys. 26 (2) (1955) 182–185.
[32] K.R. Rajagopal, L. Tao, Mechanics of Mixtures, World Scientific Publishing Company, Singapore, 1995.
[33] W.G. Gray, B.A. Schrefler, Thermodynamic approach to effective stress in partially saturated porous media, Eur. J. Mech. A. Solids 20 (4) (2001) 521–538.
[34] O. Coussy, Revisiting the constitutive equations of unsaturated porous solids using a lagrangian saturation concept, Int. J. Numer. Anal. Methods Geomech. 31 (15) (2007) 20–39.
[35] I. Vlahinic, H.M. Jennings, J.J. Thomas, A constitutive model for drying of a partially saturated porous material, Mech. Mater. 41 (3) (2009) 319–328.
[36] L.W. Morland, E.H. Lee, Stress analysis for linear viscoelastic materials with temperature variation, Society of Rheology — Transactions 4 (1960) 233–263.
[37] F. Schwarzl, A.J. Staverman, Time–temperature dependence of linear viscoelastic behavior, J. Appl. Phys. 23 (1952) 838–843.
[38] L.C.E. Struik, Physical Aging in Amorphous Polymers and Other Materials, Elsevier Scientific Pub. Co., New York, 1978.
[39] F. Rajabipour, G. Sant, J. Weiss, Interactions between shrinkage reducing admixtures (sra) and cement paste's pore solution, Cem. Concr. Res. 38 (5) (2008) 606–615.
[40] R. Defay, I. Prigogine, A. Bellemans, D.H. Everett, Surface Tension and Adsorption, John Wiley & Sons, Inc., NY, 1966.
[41] K.S. Pitzer, K.S. Pitzer (Eds.), Activity Coefficients in Electrolyte Solutions, CRC Press, Inc, Boca Raton, Florida, 1991, pp. 75–153.
[42] J. Duchesne, E.J. Reardon, Measurement and prediction of portlandite solubility in alkali solutions, Cem. Concr. Res. 25 (5) (1995) 1043–1053.
[43] C.L. Page, O. Vennesland, Pore solution composition and chloride binding capacity of silica-fume cement pastes, Mater. Struct. 16 (91) (1983) 19–25.
[44] H.J.H. Brouwers, R.J. VanEijk, Alkali concentrations of pore solution in hydrating opc, Cem. Concr. Res. 33 (2) (2003) 191–196.
[45] P. Baggio, C. Bonacina, B.A. Schrefler, Some considerations on modeling heat and mass transfer in porous media, Transp. Porous Media 28 (3) (1997) 233–251.
[46] W. Vichit-Vadakan, G.W. Scherer, Measuring permeability of rigid materials by a beam-bending method: Iii, cement paste, J. Am. Ceram. Soc. 85 (6) (2002) 1537–1544.

[47] J.R. Jaunsen, The Behavior and Capabilities of Lithium Hydroxide–Carbon Dioxide Scrubbers in a Deep Sea Environment, A862612, United States Naval Academy, Annapolis, Annapolis, MN, 1989.
[48] T.C. Wang, J.P. Krivan, Co_2 absorption capacity of new and old lithium hydroxide used in underwater life support systems, Sea Technol. 18 (12) (1977) 13–14.
[49] A. Boumiz, C. Vernet, F. Cohen Tenoudji, Mechanical properties of cement pastes and mortars at early ages, Adv. Cem. Based Mater. 3 (3–4) (1996) 94–106.
[50] O. Bernard, F.-J. Ulm, E. Lemarchand, A multiscale micromechanics-hydration model for the early-age elastic properties of cement-based materials, Cem. Concr. Res. 33 (9) (2003) 1293–1309.
[51] R.N. Swamy, Dynamic poisson's ratio of portland cement paste, mortar and concrete, Cem. Concr. Res. 1 (5) (1971) 559–583.
[52] H.F.W. Taylor, Method for prediction alkali ion concentrations in cement pore solutions, Adv. Cem. Res. 1 (1) (1987) 5–16.
[53] H.F.W. Taylor, Cement Chemistry, 2nd edThomas Telford, London, 1997.
[54] G. Pickett, The effect of change in moisture content on the creep of concrete under a sustained load, ACI Journal 38 (1942) 333–355.
[55] Z.C. Grasley, Closed form solutions for uniaxial passive restraint experiments, ACI SP 270 (2010) 17–32.